Mixed-effects Model Fitting Based on *in vivo* Data from Animal Experiments

Melánia Puskás[1,2,*], Balázs Gombos[3,4], Levente Kovács[1], and Dániel András Drexler[1]

[1]Physiological Controls Research Center, University Research and Innovation Center, Obuda University, Bécsi út 96/b, 1034 Budapest, Hungary, {puskas.melania, kovacs, drexler.daniel}@uni-obuda.hu
[2]Applied Informatics and Applied Mathematics Doctoral School, Obuda University, Bécsi út 96/b, 1034 Budapest, Hungary
[3]Drug Resistance Research Group, Hungarian Research Network, Magyar tudosok krt 2, 1117, Budapest, Hungary, gombos.balazs@ttk.hu
[4]Molecular Medicine PhD School, Semmelweis University, Üllői út 26, 1085 Budapest, Hungary
[*]Corresponding: puskas.melania@uni-obuda.hu

Abstract: The use of mixed-effects models is becoming increasingly common in the analysis of biomedical data. They are often employed for estimating physiological parameters, where we can distinguish between fixed and random effects, and they work particularly well for analyzing similar types of data. We apply mixed-effect modeling on experimental data, in which mice with breast cancer were treated with chemotherapeutic drugs. The mice are genetically identical, they had the same type of tumor, and they were treated with the same drug. The available data are the tumor volumes at specific time points and the doses of the injected drug. We fit our mathematical model to these experimental data; the parameters of that mathematical model are essentially the physiological parameters whose estimation is crucial for optimizing the therapy. To estimate the parameters, we apply a nonlinear mixed-effects model fitting to in vivo data.

Keywords: mixed-effects model, model fitting, animal experiments, parameter estimation

1 Introduction

Cancer has become a major public health problem, with the number of cases and deaths increasing every year. According to the World Health Organization (WHO), this trend is expected to continue. Although there are many treatment options for cancer, most of them are designed for the average patient and do not fully consider individual differences. Because of this, patients often experience more side effects, and their quality of life worsens during treatment [1–3]. Chemotherapy doses can be minimized with the help of optimized therapy, so side effects can also be

reduced. Reducing doses helps prevent the development of drug resistance and, last but not least, can reduce treatment costs [4, 5]. Optimized therapies are not only cost-effective but also provide an opportunity to minimize the number of clinical trials, thereby speeding up research and development. Several approaches can be used to solve the therapy optimization problem, for example, one such approach is the use of impulsive control methods [6–10], but traditional control theory can also be used [11, 12]. In this work, we focus on estimating the parameters of an *in vivo* tumor model [13, 14]. The parameters can later be used for therapy optimization algorithms.

Algorithmic therapy optimization is one of the promising tools for the future of medicine, and it forms the core of our research. The therapy optimization requires a mathematical model that can describe the effects of drugs and the dynamics of tumor growth [13, 15]. A therapy is personalized when the parameters of the mathematical model are based on the specific characteristics of the patient being treated. Estimating the unique parameters of the patients and generating optimal therapies in preclinical experiments have already been discussed in the literature [16], as these individual parameters are crucial for personalization. There are several methods for estimating the parameters of a mathematical model [17, 18]. For example, we can use model fitting using neural networks [19–22] and other search algorithms and model analysis techniques [23–25].

We use *in vivo* data from animal experiments where mice with breast cancer were treated with Doxil [26], the tumor volumes were measured, and the drug doses are known [9]. Using these *in vivo* data, we fit a mathematical model [13] that allows us to create and test personalized therapies *in silico* [27]. Model fitting plays a critical role, as it directly impacts the outcomes and effectiveness of model-based therapies. There are many solutions to the fitting problem, which also presents several challenges [28–31]. These include the limited number of tumor volume measurements and the fact that these measurements are affected by measurement error [32, 33].

Mixed-effects models are used to analyze data where observations are grouped [15], such as repeated measurements from specimens in clinical studies or biological experiments. These models are effective in handling data with both fixed and random effects [34]. Fixed effects describe the population-level relationships, and random effects describe individual variability within groups. This makes them popular in fields like pharmacokinetics, where drug concentrations and responses may vary from one patient to another due to differences in physiology, genetics, or other factors [35].

Our goal is to estimate the tumor dynamics parameters of the mathematical model using nonlinear mixed-effects model fitting. Identification of the parameters is essential for the personalization of the therapy, and with the help of the defined parameters, virtual measurements can be generated on which our therapies can be tested. We discuss the mathematical model in Section 2, and summarize the mathematics and advantages of using non-linear mixed effect models. In Section 3, we present our fitting results and examine our data from the point of view of fitting non-linear mixed effect models. We also discuss the initial value of the parameters

and the statistical tools used during the fitting. Finally, in Section 4, we present the individual fitting results of each mouse and summarize the population values of the parameters. These parameter values can be integrated into therapy optimization algorithms to create personalized treatments, and they can serve as starting values for further fitting processes when new experimental data is available.

2 Materials and Methods

2.1 Mathematical Model of Tumor Growth

There are several types of tumor models in the literature [36–38]. For example, there are tumor models that focus not only on tumor growth but also on the growth of the supporting vascular system [39], and there are other models that include drug resistance [4]. In our work, we use a mathematical model based on formal reaction kinetics [40], which deals with the drug pharmacodynamics and pharmacokinetics, and also models the dynamics of the dead tumor cells which is crucial for identification, since the measurements from the experiments contain the volume of both the living and the dead tumor cells. The tumor dynamics processes are described by the formal reaction kinetics equations [15]:

$$\mathrm{X}_1 \xrightarrow{\mathrm{a}} 2\,\mathrm{X}_1, \tag{1}$$

$$\mathrm{X}_1 \xrightarrow{\mathrm{n}} \mathrm{X}_2, \tag{2}$$

$$\mathrm{X}_2 \xrightarrow{\mathrm{w}} \mathrm{O}, \tag{3}$$

$$\mathrm{X}_1 + \mathrm{X}_3 \xrightarrow{\mathrm{b,\,ED_{50}}} \mathrm{X}_2 + \mathrm{X}_3, \tag{4}$$

$$\mathrm{X}_3 \xrightarrow{\mathrm{c}} \mathrm{O}, \tag{5}$$

$$\mathrm{X}_3 \underset{\mathrm{k_2}}{\overset{\mathrm{k_1}}{\rightleftarrows}} \mathrm{X}_4, \tag{6}$$

where (1) is tumor proliferation with rate a, (2) is the necrosis of living tumor cells independent of the drug with rate n, (3) is the washout of the dead tumor cells with washout rate w, (4) is the pharmacodynamics of the drug with maximal effect rate b and median effective dose ED_{50}, (6) is the drug transport between the central and peripheral compartment with rate constants k_1 and k_2, while (5) is the depletion of the drug with clearance c.

For the parameter estimation process, we need a mathematical model that describes the dynamics of the tumor and the drug. The parameter values of this model are estimated during the model fitting process. The mathematical model we use can be acquired from the formal reactions with a combination of mass action and Michaelis-Menten kinetics [41], resulting in a system of differential equations with four state variables [13]:

Table 1
Description and units of the model parameters.

Parameter	Description	Unit
a	proliferation rate coefficient	day^{-1}
b	drug efficiency rate coefficient	day^{-1}
c	clearance of the drug	day^{-1}
ED_{50}	median effective dose of the drug	$\text{mg}\cdot\text{kg}^{-1}$
k_1	flow rate coefficient of the drug from the central to the peripheral compartment	day^{-1}
k_2	flow rate coefficient of the drug from the peripheral to the central compartment	day^{-1}
n	necrosis rate coefficient	day^{-1}
w	washout rate coefficient of dead tumor cells	day^{-1}

$$\dot{x}_1 = (a-n)x_1 - b\frac{x_1x_3}{ED_{50}+x_3}, \tag{7}$$

$$\dot{x}_2 = nx_1 + b\frac{x_1x_3}{ED_{50}+x_3} - wx_2, \tag{8}$$

$$\dot{x}_3 = -(c+k_1)x_3 + k_2x_4 + u, \tag{9}$$

$$\dot{x}_4 = k_1x_3 - k_2x_4, \tag{10}$$

where (7) describes the growth of the living tumor, with the state variable x_1 [mm^3] representing the volume of living tumor cells as a function of time. Equation (8) describes the dead tumor, where x_2 [mm^3] represents the volume of dead tumor cells over time [15]. In (9), x_3 [$\text{mg}\cdot\text{kg}^{-1}$] shows the drug concentration in the central compartment, which, in this case, is the concentration of the drug in the blood. This equation models the behavior of the drug in the blood. Equation (10) also describes the drug concentration in the tissues, where x_4 [$\text{mg}\cdot\text{kg}^{-1}$] represents the drug level in the tissues.

The input of the system is u [$\text{mg}\cdot(\text{kg}\cdot\text{day})^{-1}$], which is the injection rate. The drug is injected into the central compartment. The output of the system is the total volume of living and dead tumor cells, denoted as y, which is the sum of the living and dead tumor cells

$$y = x_1 + x_2, \tag{11}$$

and this is the measured variable in the experiments used for model fitting in this study.

The descriptions and units of the parameters [42] of the model are summarized in Table 1. During model fitting, we estimate the values of the parameters listed in Table 1, and we fixed the pharmacokinetics parameters c, k_1, and k_2 (which will be detailed further in Section 3).

2.2 Nonlinear Mixed-effects Models

The nonlinear mixed-effects model is a general method for analyzing continuous repeated measurements taken from specimens within a specific population. This approach is particularly useful when we want to understand the average behavior of the population and the variations among specimens [43].

The main difference between linear and nonlinear mixed-effects models lies in the structure of the model and how the explanatory variables (also known as independent variables) are related to the response variables (also known as dependent variables) within the model. Nonlinear mixed-effects models are more flexible, as the relationship between the independent and dependent variables is not necessarily linear (it can be exponential, logarithmic, or any other nonlinear function) [34]. The general form of the model is

$$y_{i,j} = f(x_{i,j}, \theta) + \varepsilon_{i,j}, \tag{12}$$

where $y_{i,j}$ is the jth observation of the ith specimen (e.g., the volume of the tumor in our case) and f is a nonlinear function that describes the relationship between the dependent variable and the independent variables. Parameter $x_{i,j}$ represents the independent variables for the jth observation of the ith specimen (e.g., the dose of the drug) [44]. Parameter θ represents the parameters for the specimen, which contains the fixed and the random effects. These random effects allow the model to account for individual differences among specimens. The parameters (θ) of the specimen can be divided into two components. Fixed Parameters are valid at the population level, and random parameters are specific to individual specimens and can be written as:

$$\theta_i = \theta_{pop} + b_i, \tag{13}$$

where θ_{pop} represents the population-level parameters, these are the fixed effects that describe the average behavior characteristics of the entire population being studied and b_i is the random effect, assumed to follow a normal distribution [45]. The $\varepsilon_{i,j}$ represents the residual error for the jth observation of the ith specimen, which is the difference between the observed value ($y_{i,j}$) and the predicted value ($f(x_{i,j}, \theta)$) of the model [44, 46].

3 Model Fitting to Experimental Data

Our goal with the fitting is to determine constant parameter values in Table 1 that can describe the parameters of the population. So, we focus on a specific target group, meaning we want to estimate the parameters for this specific target group. In this case, the application of mixed effect models is a very effective and commonly used method [43]. In our research, the subjects of the experiment where we got the data from are genetically identical mice, thus, we can expect small differences among

Table 2
Initial values of the tumor dynamics parameters.

Parameters	Initial values
a [day^{-1}]	$ln(0.22)$
n [day^{-1}]	$ln(0.0005)$
b [day^{-1}]	$ln(8)$
ED_{50} [mg·kg^{-1}]	$ln(2.7183)$
w [day^{-1}]	$ln(0.004)$
$x_1(0)$ [mm^3]	$ln(50)$

their parameter values. The mixed-effects model estimates the expected value of the parameter values and models the differences between individuals as noise, so it can be used very well in our case [13, 15]. During the fitting, we accessed a dataset from 54 experimental mice. The dataset includes tumor measurement time points, injection time points, the measured volume of the tumor, the amount of the injected dose, and the unique ID for each mouse. The mice and tumor type can be found in the work of Füredi et al. [26], and the experimental setup is detailed in the works of Kovács et al. [9, 47].

Fitting the parameters is actually based on the comparison of two curves. We have the observed measurements, which, in our case, are the measured tumor volumes, and the predicted tumor volume values obtained during fitting, which are obtained by the estimated parameters and by our mathematical model. The aim of the fitting is to minimize the difference between the two curves. We can examine the deviation of the two curves with different indicators. In our work, we examined the individual weighted residual (IWRES) error, which weights the deviations (residuals) between the observed values (DV) and the values predicted (IPRED) by the model with the variance of the measurement data ($\hat{\sigma}$) [48]:

$$\mathrm{IWRES}_i = \frac{\mathrm{DV}_i - \mathrm{IPRED}_i}{\hat{\sigma}_i}, \tag{14}$$

where i denotes the index of the specimen. The IWRES standardizes differences between observations so that different individuals become comparable. The closer this value (14) is to zero, the smaller the error, and the closer the fitted curve follows the observed data [49]. So the IWRES value weights the residual based on inter-individual variability, which allows residuals to more accurately reflect variation at different levels (e.g., population and individual). In general, individual residual values (IRES) can also be used, but they do not take weighting into account, so they do not always adequately reflect individual-specific differences and variability, so we chose the weighted version for the evaluation of results (the evaluation is detailed in Section 4). IWRES can also be used to identify individuals for whom the model fits poorly, likely because they differ from the majority of mice.

In order to estimate the parameters, the algorithm requires initial values to start the search. One of the main drawbacks of search algorithms is the need to select appropriate initial values from which the search begins. For the fitting process,

Table 3
Fixed pharmacodynamics and pharmacokinetics values.

Parameters	Constant values
c [day^{-1}]	1.8211
k_1 [day^{-1}]	14.0080
k_2 [day^{-1}]	136.2781

the initial parameter values were set empirically during the first run, based on our previous work [22]. After the first run, we always examined the expected value and standard deviation of the fitted parameters, and the next fitting was based on these. Table 2 contains the initial values from which the search for the parameters was started and the best results were obtained. Parameter $x_1(0)$ represents the initial living tumor volume, which was estimated during the fitting.

Based on the previous analysis of our mathematical model, it was established that the parameters c, k_1, and k_2 have a small influence on the output of the model [50], so they are difficult to estimate. These parameters were fixed in this work, so their value was not estimated. The fixed values, which were estimated based on our previous work [9, 13, 20], are summarized in Table 3.

The measurement data were processed, and the fitting results were evaluated in Matlab, while the nonlinear mixed-effect model fitting was done in RStudio with *nlmixr2* package [51, 52]. This package is commonly used to fit non-linear mixed-effect (NLME) models, mainly for pharmacokinetic (PK), and pharmacodynamic (PD) models, but also for modeling other mixed-effect models [53]. When using the package, we used the SAEM (Stochastic Approximation Expectation-Maximization) estimation algorithm. This is a popular method for fitting nonlinear mixed-effects models, as well as in a pharmacometric context. The SAEM algorithm uses an iterative approach based on the estimation of distributions and the evaluation of data [54].

4 Results

Parameter fitting was performed on the full dataset, which comprised 54 experimental mice. The IWRES values based on (14) were examined in all specimens, the results of which can be seen in Figures 1 and 2, both figures showing the results for 27 mice. In these figures, the red horizontal line is the median of the data, the blue rectangles show the range where 25%-75% of the data are (so these are the first (Q1) and third (Q3) quartiles), the whiskers typically extend to the data points that are within 1.5 times the IQR (IQR = Q3-Q1) and these are not considered as outliers, while red crosses indicate outliers. The x-axis indicates the ID of the mice and the y-axis the individual weighted residuals (IWRES). Examining Figures 1 and 2, it is easy to recognize the possibly worst-fitting individuals. In our case, the goal is that the boxes belonging to the individuals are as small as possible and

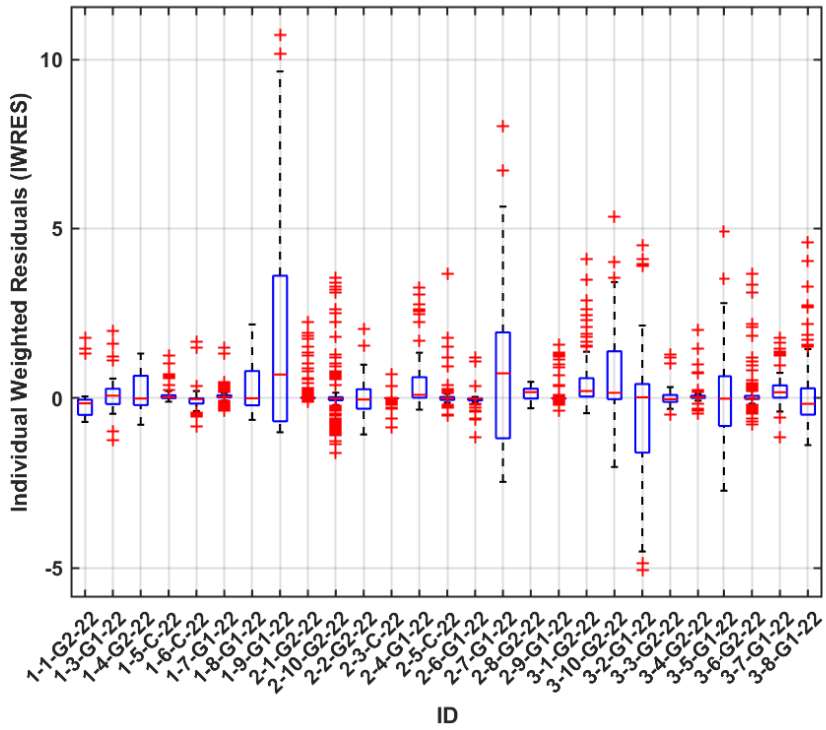

Figure 1
Individual weighted residuals (IWRES) of the first 27 specimen, which can be used to examine the goodness of fit.

the medians (red line) are located close to zero, since in this case, the fit is more accurate.

Figure 1 clearly shows that for specimens 1-9-G1-22, 2-7-G1-22 and 3-2-G1-22, the error moves over a larger interval, and each specimen has some outlier values. The medians, on the other hand, are around zero for all individuals, and except for a few cases, the boxes are also small, which indicates the movement of the errors on a small interval, so overall a good fit can be concluded.

In Figure 2, the results are similar to those seen in the individuals shown in Figure 1. However, in this case, slightly more individuals exhibit larger boxes in the boxplot of residuals, indicating a greater variability in the errors. This is particularly evident for individuals 4-1-G1-22, 4-2-G2-22, 5-10-G1-22, and 5-6-G1-22, where the interquartile range of the residuals is the largest. Despite this increased spread, the medians of the residuals still mostly remain close to zero, generally falling within the interval of -2 to 2, which suggests the absence of a considerable bias in the fit.

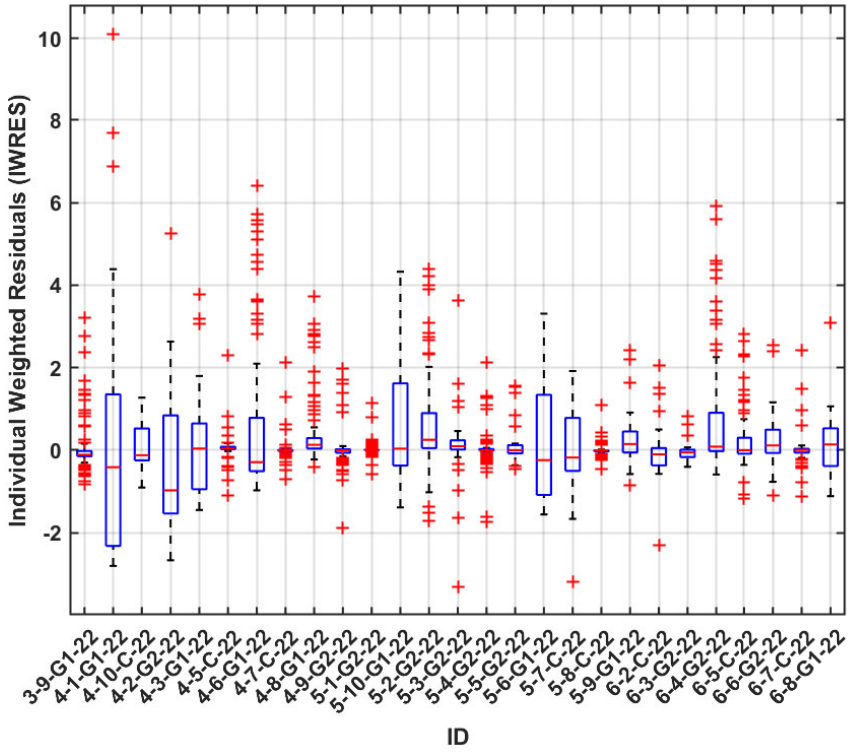

Figure 2
Individual weighted residuals (IWRES) of the second 27 specimens, which can be used to examine the goodness of fit.

Figures 3 and 4 show the fitting results for each mouse. Each mouse can be distinguished based on the unique IDs, and in each figure, the x-axis represents time, the left y-axis represents the tumor volumes and the right y-axis represents the doses. The figures show the tumor volume measurements (observed measurements with blue curve) of mice from the same population and the estimated tumor volume (individual prediction with red curve) fitted based on the nonlinear mixed-effect model. The green vertical lines indicate the injection days and the doses.

Figure 3 shows that the individual prediction (red curve) does not fit well with the observed measurements (blue curve) of the 1-9-G1 and 3-2-G1-22 mice, and that in the case of the 2-7-G1-22 mouse. In Figure 4, we can also see the 4-1-G1-22 mouse, for which we concluded based on Figure 2 that we might not get a nice fit and that this curve did not fit properly. However, it can be stated that, overall, we obtained nice fitting results.

We examined the IWRES results at the population level; it is summarized in Table

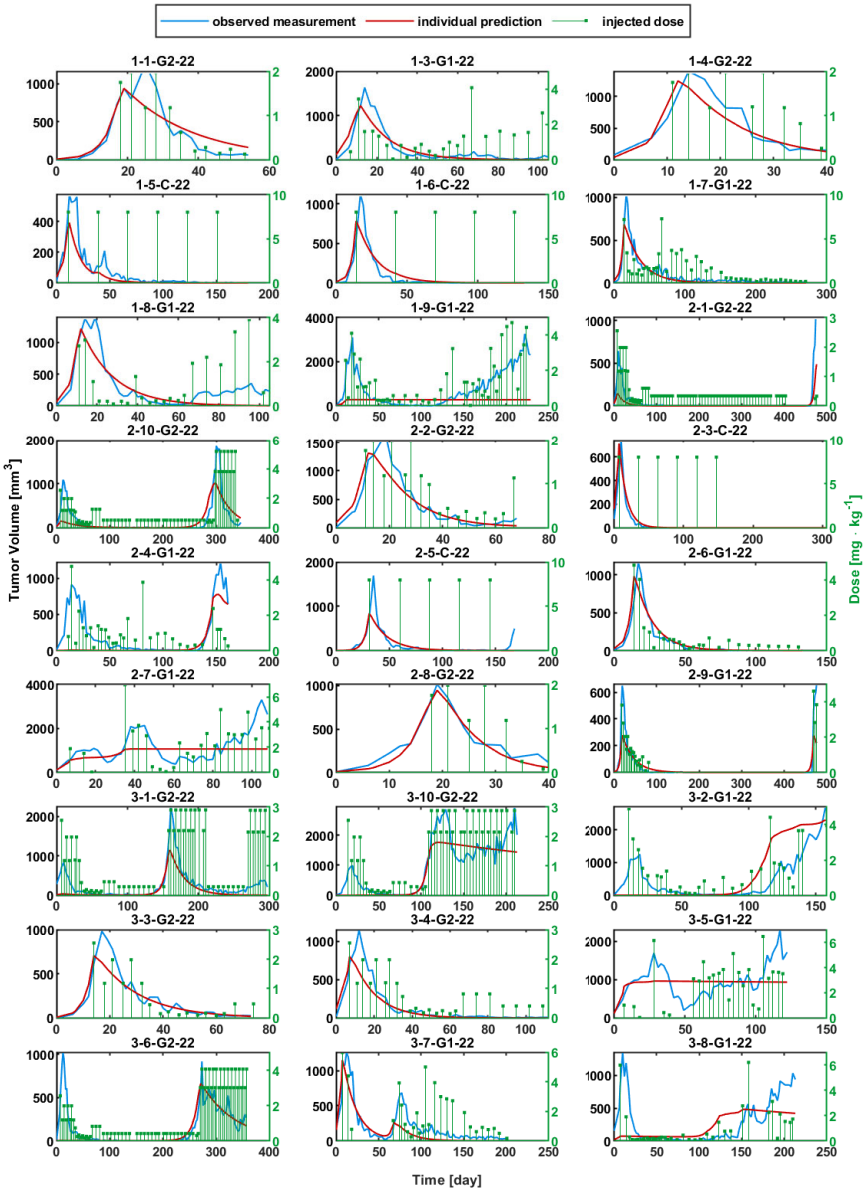

Figure 3

The tumor volume measurements [mm^3] (observed measurements with the blue curve) of mice and the estimated tumor volume [mm^3] (individual prediction with the red curve) fitted based on the nonlinear mixed-effect model. The green vertical lines indicate the day of injection and the dose in $mg \cdot kg^{-1}$.

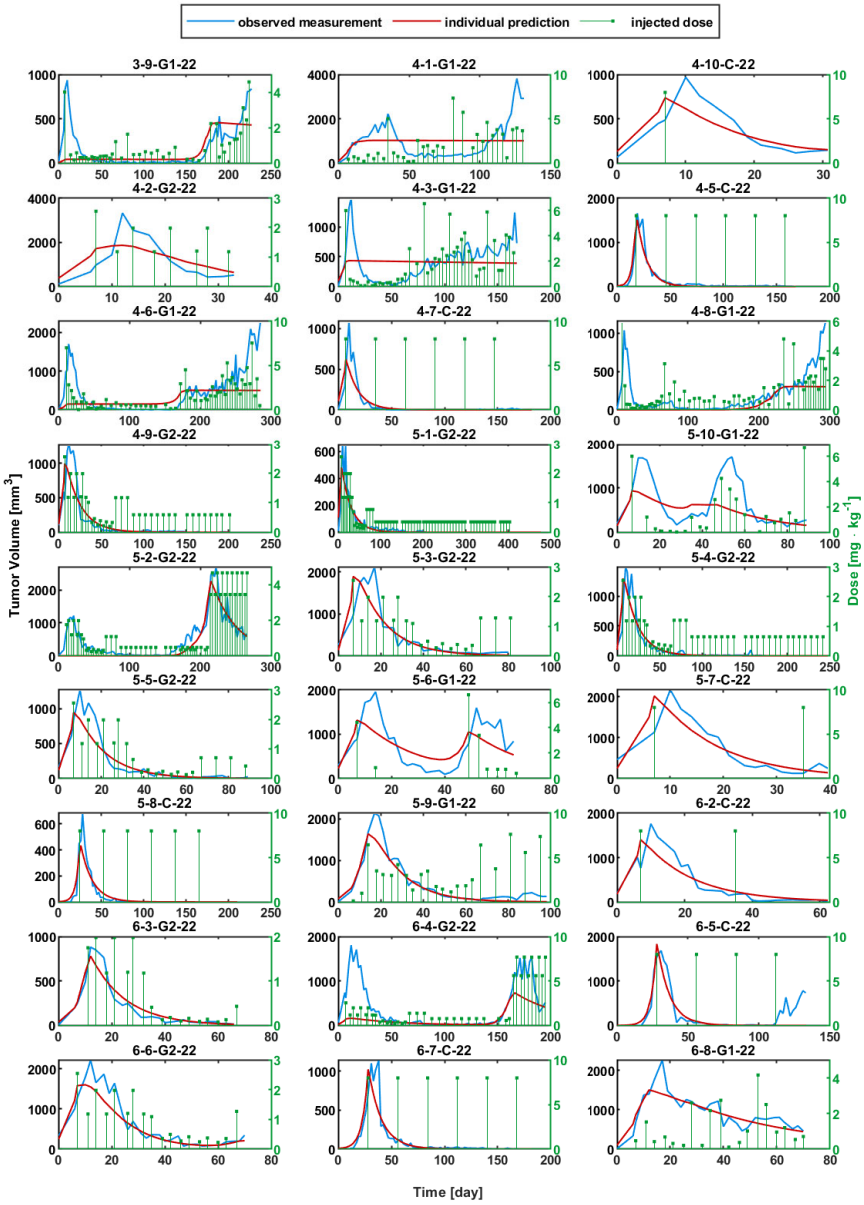

Figure 4
The tumor volume measurements [mm^3] (observed measurements with the blue curve) of mice and the estimated tumor volume [mm^3] (individual prediction with the red curve) fitted based on the nonlinear mixed-effect model. The green vertical lines indicate the day of injection and the dose in $mg \cdot kg^{-1}$.

Table 4
Statistical data for the individual weighted residuals (IWRES) at the population level.

	Minimum	Q1	Median	Mean	Q3	Maximum
IWRES	-5.0695	-0.0559	-4.24e-10	0.2102	0.1727	10.7197

Table 5
Statistical indicators of fitted parameters at the population level.

Parameters	a	n	b	ED_{50}	w	x_{10}
Minimum	0.1694	3.47e-04	4.2296	0.5408	4.40e-05	0.0034
Median	0.2435	4.71e-04	9.2740	1.4489	0.0431	24.3271
Mean	0.2435	4.74e-04	9.3849	1.8643	0.0456	52.4025
Maximum	0.3807	6.03e-04	14.5180	7.2009	0.1466	383.0802
SD	0.0430	4.86e-05	2.1989	1.3038	0.0328	61.4707

4. This also shows that, e.g., the median is also close to zero at the population level, the mean is also small and the quartiles also have small values, which is definitely positive information for the success of the fit, but in any case, in the future, grouping based on tumor dynamics may further clarify this result.

The parameters we were looking for were obtained by the fitted curves, which are also summarized at the population level in Table 5. The header of the table shows the fitted model parameters (a, n, b, ED_{50}, w) and the fitted initial living tumor volume ($x_1(0)$). We examined the minimum and maximum values, the median, the average, and the standard deviation (SD) for each parameter. According to Table 5, the most reliable estimate was obtained for parameter n, as it has the smallest standard deviation, followed by parameters a and w. Moreover, the median, mean, minimum, and maximum values are all closely aligned. Overall, the statistical measures suggest that the parameter values vary only minimally between individuals, indicating a successful fit. The only exception is the initial living tumor volume $x_1(0)$, which exhibits a larger standard deviation and greater variability in its statistical indicators. This is expected, as the mice started the experiment with different initial tumor volumes.

Conclusion

We estimated the parameters of a mathematical model describing tumor growth under chemotherapy using nonlinear mixed-effects model fitting. The dataset consisted of tumor volume measurements from in vivo mouse experiments along with the corresponding administered doses. The pharmacokinetic parameters (three out of the eight estimable parameters) were fixed based on values reported in our previous studies and were not re-estimated. We also estimated the initial volume of living tumor tissue. The evaluation of the six estimated parameters confirmed that the model parameters can be reliably estimated using this fitting approach. The results support our assumption that inter-individual variability among the mice is small, and the fitting was successful both at the individual and population levels. In future work, it will be important to cluster tumor growth curves based on their

dynamics [20], in order to define more homogeneous groups. For such groups, model fitting could yield more accurate and specific parameter estimates.

We currently estimate fixed parameter values, but based on the experimental data, we have already concluded that these physiological parameters may change over time. In the cases where the model did not fit well for certain mice, we observed that after a period of remission (tumor reduction), the tumor suddenly regrew, indicating relapse. The model had difficulty describing this because it assumes constant parameters, while the tumor growth dynamics are likely to change over time. As a further improvement step, it might be worthwhile to examine this with a fitting method where the fitting is performed in stages. In this way, parameter changes can also be tracked, so the estimation can be more realistic and accurate. The current result can be well integrated into many research since therapy optimization algorithms can use these parameter values during the generation of the unique therapy or can be used to carry out *in silico* experiments. In addition, these parameter values can be additional starting values during a further fitting process if new experimental results are obtained. In our future work, we would like to further refine our model with a deeper analysis of the differences between individual mice, enabling a more precise parameter estimation of the tumor model.

Acknowledgment

This project has been supported by the Hungarian National Research, Development and Innovation Fund of Hungary, financed under the TKP2021-NKTA-36 funding scheme. The work of Dániel András Drexler was supported by the Starting Excellence Researcher Program of Obuda University, Budapest Hungary. Melánia Puskás is also with the Obuda University, Applied Informatics and Applied Mathematics Doctoral School, Budapest, Hungary. Melánia Puskás was supported by the 2024-2.1.1 University Research Scholarship Program of the Ministry for Culture and Innovation from the source of the National Research, Development and Innovation Fund. Melánia Puskás acknowledges the support of the National Talent Program under the NTP-HHTDK-24-0078 project. This research was partially supported by the European Union (EU HORIZON-MSCA-2023-SE-01-01) and the Hungarian NRDI program (2020-2.1.1-ED-2024-00346) within the DSYREKI: Dynamical Systems and Reaction Kinetics Networks project.

References

[1] C. de Martel, D. Georges, F. Bray, J. Ferlay, and G. M. Clifford. Global burden of cancer attributable to infections in 2018: a worldwide incidence analysis. *The Lancet Global Health*, 8(2):e180–e190, 2020.

[2] J. Ferlay, M. Colombet, I. Soerjomataram, D. M. Parkin, M. Piñeros, A. Znaor, and F. Bray. Cancer statistics for the year 2020: An overview. *International Journal of Cancer*, 2021.

[3] V. Zah, A. Burrell, C. Asche, and Z. Zrubka. Paying for digital health interventions – what evidence is needed? *Acta Polytechnica Hungarica*, 19(9):179–199, 2022.

[4] J. M. Greene, J. L. Gevertz, and E. D. Sontag. Mathematical approach to differentiate spontaneous and induced evolution to drug resistance during cancer treatment. *JCO Clinical Cancer Informatics*, (3):1–20, 2019.

[5] F. Cacace, V. Cusimano, and P. Palumbo. Optimal impulsive control with application to antiangiogenic tumor therapy. *IEEE Transactions on Control Systems Technology*, 28(1):106–117, Jan 2020.

[6] D. A. Drexler and L. Kovács. Optimization of impulsive discrete-time tumor chemotherapy. In *Proceedings of the 2019 IEEE 1st International Conference on Societal Automation.*, 2019.

[7] D. A. Drexler, J. Sápi, and L. Kovács. H control of nonlinear systems with positive input with application to antiangiogenic therapy∗∗this project has received funding from the european research council (erc) under the european union's horizon 2020 research and innovation programme (grant agreement no 679681). *IFAC-PapersOnLine*, 51(25):146–151, 2018. 9th IFAC Symposium on Robust Control Design ROCOND 2018.

[8] B. Péceli, D. A. Drexler, and L. Kovács. Optimal scheduling of low-dose metronomic chemotherapy: an in-silico analysis. In *2020 IEEE 15th International Conference of System of Systems Engineering (SoSE)*, pages 411–416, 2020.

[9] L. Kovács, T. Ferenci, B. Gombos, A. Füredi, I. Rudas, G. Szakács, and D. A. Drexler. Positive impulsive control of tumor therapy—a cyber-medical approach. *IEEE Transactions on Systems, Man, and Cybernetics: Systems*, 54(1):597 – 608, 2024.

[10] D. A. Drexler, J. Sápi, and L. Kovács. Positive control of a minimal model of tumor growth with bevacizumab treatment. In *2017 12th IEEE Conference on Industrial Electronics and Applications (ICIEA)*, pages 2084–2087, 2017.

[11] J. Klamka, H. Maurer, and A. Swierniak. Local controllability and optimal control for a model of combined anticancer therapy with control delays. *Mathematical Biosciences and Engineering*, 14(1):195–216, 2017.

[12] F. S. Lobato, V. S. Machado, and V. Steffen. Determination of an optimal control strategy for drug administration in tumor treatment using multi-objective optimization differential evolution. *Computer Methods and Programs in Biomedicine*, 131:51 – 61, 2016.

[13] D. A. Drexler, T. Ferenci, A. Füredi, G. Szakács, and L. Kovács. Experimental data-driven tumor modeling for chemotherapy. In *Proceedings of the 21st IFAC World Congress*, pages 16466–16471, 2020.

[14] M. Puskás and D. A. Drexler. Tumor model parameter estimation for therapyoptimization using artificial neural networks. In *IEEE International Conference on Systems, Man, and Cybernetics - 2021*, pages 1254–1259, 2021.

[15] D. A. Drexler, T. Ferenci, A. Lovrics, and L. Kovács. Tumor Dynamics Modeling based on Formal Reaction Kinetics. *Acta Polytechnica Hungarica*, 16:31–44, 2019.

[16] B. Gergics, F. Vajda, M. Puskás, A. Füredi, and D. A. Drexler. Mathematical modeling of phototoxicity during fluorescent imaging of tumor spheroids. In *2023 IEEE 27th International Conference on Intelligent Engineering Systems (INES)*, pages 000291–000296, 2023.

[17] O. Nelles. *Nonlinear System Identification: From Classical Approaches to Neural Networks and Fuzzy Models*. Springer, Berlin, Heidelberg, 2001.

[18] L. Ljung. *System Identification: Theory for the User*. Prentice Hall, Upper Saddle River, NJ, 2nd edition, 1999.

[19] G. Quaranta, W. Lacarbonara, and S. F. Masri. A review on computational intelligence for identification of nonlinear dynamical systems. *Nonlinear Dynamics*, 99:1709–1761, 2020.

[20] L. Kisbenedek, M. Puskás, L. Kovćs, and D. A. Drexler. Clustering-based parameter estimation of a tumor model. In *SISY 2023 IEEE 21st International Symposium on Intelligent Systems and Informatics*, pages 43–48, 2023.

[21] L. Bertolaccini, P. Solli, A. Pardolesi, and A. Pasini. An overview of the use of artificial neural networks in lung cancer research. *Journal of Thoracic Disease*, 9(4):924–931, 2017.

[22] M. Puskás, B. Gergics, A. Ládi, and D. A. Drexler. Parameter estimation from realistic experiment scenario using artificial neural networks. In *2022 IEEE 16th International Symposium on Applied Computational Intelligence and Informatics (SACI)*, pages 161–168, 2022.

[23] L. Wang, J. Cao, J. O. Ramsay, D. M. Burger, C. J. L. Laporte, and J. K. Rockstroh. Estimating mixed-effects differential equation models. *Statistics and Computing*, 24:111–121, 2014.

[24] M. Kühleitner, N. Brunner, W. G. Nowak, et al. Best fitting tumor growth models of the von bertalanffy-pütter type. *BMC Cancer*, 19:683, 2019.

[25] G. M. Palmer, C. Zhu, T. M. Breslin, F. Xu, K. W. Gilchrist, and N. Ramanujam. Monte carlo-based inverse model for calculating tissue optical properties. part ii: Application to breast cancer diagnosis. *Appl. Opt.*, 45(5):1072–1078, Feb 2006.

[26] A. Füredi, K. Szebényi, S. Tóth, M. Cserepes, L. Hámori, V. Nagy, E. Karai, P. Vajdovich, T. Imre, P. Szabó, D. Szüts, J. Tóvári, and G. Szakács. Pegylated liposomal formulation of doxorubicin overcomes drug resistance in a genetically engineered mouse model of breast cancer. *Journal of Controlled Release*, 261:287–296, 2017.

[27] M. F. Dömény, M. Puskás, L. Kovács, and D. A. Drexler. Population-based chemotherapy optimization using genetic algorithm. In *2023 IEEE 21st*

International Symposium on Intelligent Systems and Informatics (SISY), pages 23–28. IEEE, September 2023.

[28] M. Puskás, B. Gergics, L. Kovács, and D. A. Drexler. Tumor volume measurements in animal experiments: Current approaches and their limitations. In W. Zamojski, J. Mazurkiewicz, J. Sugier, T. Walkowiak, and J. Kacprzyk, editors, *System Dependability - Theory and Applications*, pages 206–217, Cham, 2024. Springer Nature Switzerland.

[29] B. Gergics and D. A. Drexler. Mathematical modeling of tumor based on in vitro and in vivo data, and in vitro to in vivo extrapolation and its challenges: a literature review. In *2023 IEEE 23rd International Symposium on Computational Intelligence and Informatics (CINTI)*, pages 000291–000298, 2023.

[30] V. Patakvölgyi, L. Kovács, and D. A. Drexler. Artificial neural networks based cell counting techniques using microscopic images: A review. In *2024 IEEE 18th International Symposium on Applied Computational Intelligence and Informatics (SACI)*, pages 327–332, 2024.

[31] D. Morton, L. Connolly, L. Groves, K. Sunderland, T. Ungi, A. Jamzad, M. Kaufmann, K. Ren, J. F. Rudan, G. Fichtinger, and P. Mousavi. Development of a research testbed for intraoperative optical spectroscopy tumor margin assessment. *Acta Polytechnica Hungarica*, 20(8):155–173, 2023.

[32] M. Puskás, B. Gergics, B. Gombos, A. Füredi, G. Szakács, L. Kovács, and D. A. Drexler. Noise modeling of tumor size measurements from animal experiments for virtual patient generation. In *2023 IEEE 27th International Conference on Intelligent Engineering Systems (INES)*. IEEE, July 2023.

[33] M. Puskás and D. A. Drexler. Modeling the error of caliper measurements in animal experiments. *IEEE Access*, 13:54836–54852, 2025.

[34] J. C. Pinheiro and D. M. Bates. *Mixed-Effects Models in S and S-PLUS*. Springer-Verlag, New York, 2000.

[35] M. J. Lindstrom and D. M. Bates. Nonlinear mixed effects models for repeated measures data. *Biometrics*, 46(3):673–687, 1990.

[36] P. M. Altrock, L. L. Liu, and F. Michor. The mathematics of cancer: integrating quantitative models. *Nature Reviews. Cancer*, 15(12):730–745, 2015.

[37] A. Borri, M. d'Angelo, L. D'Orsi, M. Pompa, S. Panunzi, and A. D. Gaetano. Stochastic modeling of glioblastoma spread: a numerical simulation study. In *21st International Multidisciplinary Modeling & Simulation Multiconference*, Tenerife, Spain, September 18–20 2024. Submitted on May 15, 2024.

[38] M. Pompa, S. Panunzi, A. Borri, and A. D. Gaetano. An agent-based model of glioblastoma infiltration. In *2023 IEEE 23rd International Symposium on Computational Intelligence and Informatics (CINTI)*, pages 383–390, 2023.

[39] P. Hahnfeldt, D. Panigrahy, J. Folkman, and L. Hlatky. Tumor development under angiogenic signaling: A dynamical theory of tumor growth, treatment response, and postvascular dormancy. *Cancer Research*, 59:4770–4775, 1999.

[40] J. Tóth, A. L. Nagy, and D. Papp. *Reaction kinetics: exercises, programs and theorems*. Springer, 2018.

[41] D. A. Drexler, J. Sápi, and L. Kovács. Modeling of tumor growth incorporating the effects of necrosis and the effect of bevacizumab. *Complexity*, pages 1–11, 2017.

[42] M. F. Doméný, M. Puskás, L. Kovács, T. T. Mac, and D. A. Drexler. Detecting critical supervision intervals during in silico chemotherapy treatments. *Acta Polytechnica Hungarica*, 21(9):247–261, 2024.

[43] M. Davidian. *Nonlinear Mixed Effects Models*, pages 947–950. Springer Berlin Heidelberg, Berlin, Heidelberg, 2011.

[44] R. Drikvandi. Nonlinear mixed-effects models for pharmacokinetic data analysis: assessment of the random-effects distribution. *Journal of Pharmacokinetics and Pharmacodynamics*, 44(3):223–232, June 2017.

[45] M. Davidian and D. M. Giltinan. Nonlinear models for repeated measurement data: An overview and update. *Journal of Agricultural, Biological, and Environmental Statistics*, 8(4):387–419, 2003.

[46] E. F. Vonesh and V. M. Chinchilli. *Linear and Nonlinear Models for the Analysis of Repeated Measurements*. CRC Press, 1st edition, 1997. Nonlinear models.

[47] L. Kovács, B. Czakó, M. Siket, T. Ferenci, A. Füredi, B. Gombos, G. Szakács, D. A. Drexler, and Q. Wang. Experimental closed-loop control of breast cancer in mice. *Complexity*, 2022, January 2022.

[48] M. M. A. Ibrahim, R. Nordgren, M. C. Kjellsson, and M. O. Karlsson. Model-based residual post-processing for residual model identification. *AAPS PharmSciTech*, 20(81), 2018.

[49] J. H. Proost. Combined proportional and additive residual error models in population pharmacokinetic modelling. *European Journal of Pharmaceutical Sciences*, 109:S78–S82, 2017. Special issue in honour of Professor Meindert Danhof.

[50] M. Siket, G. Eigner, and L. Kovács. Sensitivity and identifiability analysis of a third-order tumor growth model. In *2020 IEEE 15th International Conference of System of Systems Engineering (SoSE)*, pages 417–422, 2020.

[51] M. Fidler. *nlmixr2: Nonlinear Mixed Effects Models in Population PK/PD*, 2024. R package version 3.0.0.

[52] M. Fidler, J. Wilkins, R. Hooijmaijers, T. Post, R. Schoemaker, M. Trame, Y. Xiong, and W. Wang. Nonlinear mixed-effects model development

and simulation using nlmixr and related r open-source packages. *CPT: Pharmacometrics & Systems Pharmacology*, 8(9):621–633, sep 2019.

[53] R. Schoemaker, M. Fidler, C. Laveille, J. Wilkins, R. Hooijmaijers, T. Post, M. Trame, Y. Xiong, and W. Wang. Performance of the saem and focei algorithms in the open-source, nonlinear mixed effect modeling tool nlmixr. *CPT: Pharmacometrics & Systems Pharmacology*, 8(12):923–930, dec 2019.

[54] E. Comets, A. Lavenu, and M. Lavielle. Parameter estimation in nonlinear mixed effect models using saemix, an r implementation of the saem algorithm. *Journal of Statistical Software*, 80(3):1–41, 2017.